SF2A 2024
M. Béthermin, K. Baillié, N. Lagarde, J. Malzac, R.-M. Ouazzani, J. Richard, O. Venot, A. Siebert (eds)

PARTICLE ACCELERATION AND MAGNETIC FIELD AMPLIFICATION IN THE JET TERMINATION SHOCKS AT ALL SCALES

A. Araudo[1]

Abstract. Shocks in highly supersonic astrophysical jets at all scales are excellent scenarios for the study of non-thermal processes. In this contribution we present our recent findings on the processes of diffusive shock acceleration and magnetic field amplification in jets from massive young stellar objects and powerful radiogalaxies. In the former case, the coexistence of an adiabatic and a radiative shock represents a promising scenario for the enhancement of the gamma-ray emission. In the latter case, we find that the maximum energy of electrons accelerated in the hotspots of powerful radiogalaxies cannot be constrained by synchrotron losses as is usually assumed, unless the jet density is unreasonably large. We present a mechanism for limiting the maximum energy of electrons to the observed values, and show that the same constraint applies also to protons. This will result in severe constraints on the acceleration of ultra-high-energy cosmic rays in the hotspots of powerful radiogalaxies.

Keywords: shocks, jets, radiogalaxies, star formation, cosmic rays, gamma rays

1 Introduction

Bipolar ejection of collimated plasma from the inner regions of the accretion disc around a central object is a common process in Nature. Supersonic jets produce shocks where particles are accelerated through Diffusive Shock Acceleration (DSA). Magnetic turbulence near the shock allows particles to diffuse back and forth across the shock front, gaining energy at each crossing cycle (Axford et al. 1977; Krymskii 1977; Bell 1978; Blandford & Ostriker 1978). The maximum energy that particles can achieve is usually determined by comparing radiative losses with the acceleration timescale. This approach can lead to wrong conclusions when other aspects of the plasma are overlooked.

Based on theoretical considerations and observational analysis of a sample of well observed hotspots, Araudo et al. (2016, 2018) demonstrate that the mean-free path required for the electrons' maximum energy to be constrained by synchrotron cooling is larger than the upper limit imposed by plasma physics. As a conclusion, synchrotron losses do not constrain the maximum energy of electrons accelerated in the jet termination shocks of powerful radiogalaxies, at least the jet density in the termination region in unreasonable large. The maximum energy to which particles can be accelerated in the jet termination shocks of powerful radiogalaxies is probably determined by a more fundamental limit related with i) the steepness of the CR spectrum that excite plasma instabilities, ii) the small scale of the turbulence, and iii) the perpendicularity of the shock, making relativistic plasmas unable to accelerate particles up to energies much higher than 1 PeV (Bell et al. 2018).

In our Galaxy, the termination region of jets from Massive Young Stellar Objects (MYSO) with velocities of $\sim$300-1000 km s^{-1} are, in several cases, synchrotron emitters. In Araudo et al. (2021) we show that the mG magnetic fields inferred from the synchrotron emission must be the result of field amplification by the Non-Resonant Hybrid (NRH) instability (Bell 2004, 2005). In addition, the escape of particles upstream of the shock limits the maximum energy of the protons driving the instability to 1 TeV.

These upper limits on the maximum proton energies have important implications for the acceleration of Ultra-High Energy Cosmic Rays (UHECRs) in the hotspots of powerful radiogalaxies and for the potential gamma-ray emission from MYSO jets. In this contribution we review our studies of particle acceleration and magnetic field amplification in relativistic and non-relativistic shocks, where we combine high-resolution radio data with plasma physics.

[1] Extreme Light Infrastructure ERIC, ELI Beamlines Facility, Za Radnicí 835, CZ-25241 Dolní Břežany, Czech Republic

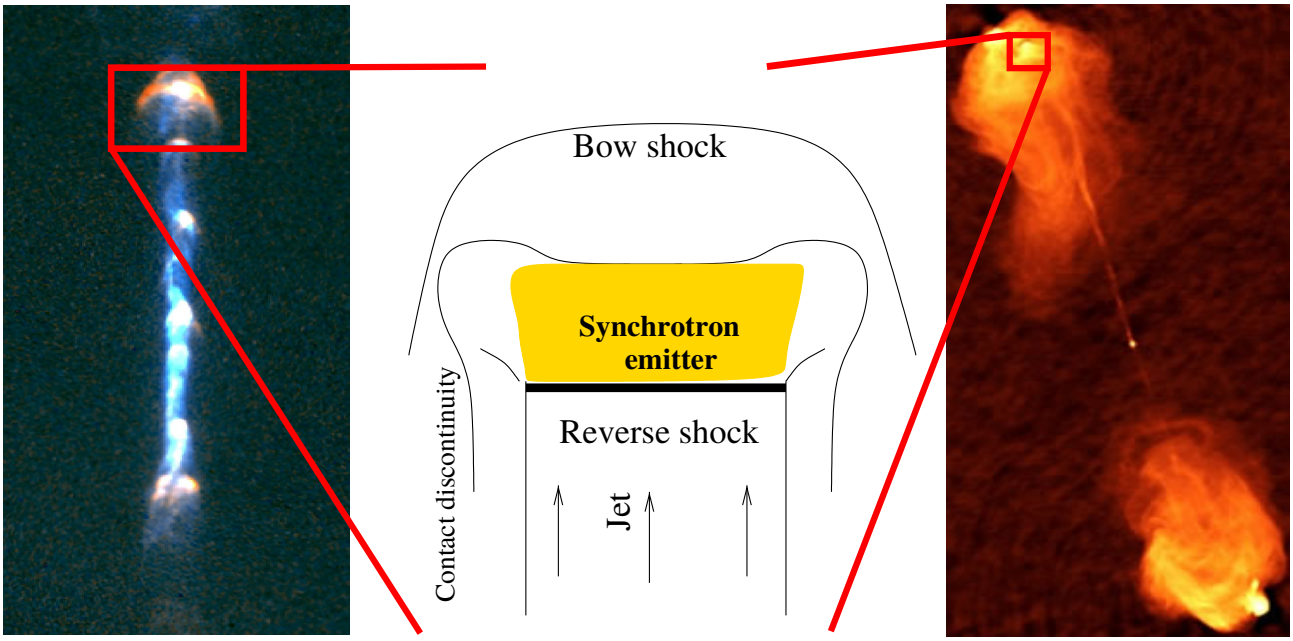

Fig. 1. Left: Jet form a young stellar object. **Middle:** Sketch of the jet termination shocks. **Right:** Radiogalaxy Cygnus A.

2 Magnetic field amplification in the jet termination shocks

The jet termination region is characterized by a double shock structure separated by a contact discontinuity, as it is sketched in the middle panel of Figure 1. The downstream region of the jet reverse shock, where electrons accelerated by the shock emit synchrotron radiation. The synchrotron emissivity per unit frequency ν emitted by a source with volume V_e located at distance d from Earth is $\epsilon_{\mathrm{syn},\nu} = 4\pi d^2 S_\nu / V_\mathrm{e}$, where S_ν is the flux at frequency ν. By setting $U_\mathrm{e,tot} = B^2_\mathrm{eq,e}/(8\pi)$ we find that the magnetic field in equipartition with relativistic electrons is

$$\frac{B_\mathrm{eq,e}}{\mathrm{mG}} \approx (1.2\xi_\mathrm{K}(s))^{\frac{2}{s+5}} \left(\frac{f_e}{10}\right)^{\frac{2}{s+5}} \left(\frac{\epsilon_{\mathrm{syn},\nu}}{10^{-30}\ \mathrm{erg\ s^{-1}\ cm^{-3}\ Hz^{-1}}}\right)^{\frac{2}{s+5}} \left(\frac{\nu}{\mathrm{GHz}}\right)^{\frac{s-1}{s+5}}, \tag{2.1}$$

where $U_\mathrm{e,tot}$ is the energy density in non-thermal electrons following a power-law distribution with index $s = 2\alpha + 1$ and α is the radio spectral index. $f_{e,p} = (m_{e,p}c^2)^{2-s}/(s-2)$ when $s > 2$ and $\xi_\mathrm{K}(s)$ is described in Appendix A in Araudo et al. (2021).

Contrary to electrons, we cannot estimate the amount of non-thermal protons in the jet termination shocks from observations. We constrain the energy density in relativistic protons as $U_{p,\mathrm{tot}} = aU_{e,\mathrm{tot}}$, where $a \geq 0$ (see Araudo et al. 2021, for more details). The magnetic field in equipartition with non-thermal electrons and protons is $B_\mathrm{eq} = \sqrt{1+a}B_\mathrm{eq,e}$. By considering the values in Table 1 we obtain that the average equipartition magnetic field is $\langle B_\mathrm{eq}\rangle = 7.25$ mG and $53.8\,\mu$G, in the jet termination region of MYSO (Araudo et al. 2021) and in the hotspots (Araudo et al. 2016), respectively. These values are larger than those expected in these sources, indicating that the magnetic field is locally amplified.

2.1 Non-resonant hybrid instabilities

We define the total proton acceleration efficiency $\eta_\mathrm{p,tot} = U_\mathrm{p,tot}/U_\mathrm{kin}$, where U_kin is the jet kinetic energy density. These protons can drive a current that combined with small perturbations present in the magnetic field can excite non-resonant waves (Bell 2004). The acceleration efficiency η_p of protons with energy E_p is defined as $\eta_p = \eta_{p,\mathrm{tot}}/f_p$. The current $j_\mathrm{p} = n_\mathrm{p} e\, v_\mathrm{sh}$ of relativistic protons with energy E_p and a number density $n_\mathrm{p} = \eta_\mathrm{p} U_\mathrm{kin}/E_p$ can drive MHD turbulence due to the force $\mathbf{j_p} \times \mathbf{B}$ added in the momentum equation (Bell 2004, 2005). The parameter η_p represents the fraction of the kinetic energy imparted into protons with energy

Table 1. Average values from a sample of eleven MYSO and eight hotspots observed in radio.

	MYSO	Hotspots
Radio spectral index	$\langle\alpha\rangle = 0.55$	$\langle\alpha\rangle = 0.79$
Synchrotron emissivity	$\langle\epsilon_{\rm syn,\nu}\rangle = 2\times10^{-30}$ erg cm^{-3} s^{-1}Hz^{-1}	$\langle\epsilon_{\rm syn,\nu}\rangle = 9\times10^{-36}$ erg cm^{-3} s^{-1}Hz^{-1}
Equipartition magnetic field	$\langle B_{\rm eq}\rangle = 7.25$ mG	$\langle B_{\rm eq}\rangle = 53.8\,\mu$G

$E_{\rm p}$ driving the instabilities. The maximum growth rate of the Bell instability excited by protons with energy $E_{\rm p}$ and carrying a current of strength $j_{\rm p}$ is $\Gamma_{\rm max} = 0.5(j_{\rm p}/c)\sqrt{\pi/n_{\rm j}\,m_{\rm i}}$.

In the linear regime of the NRH instability the magnetic field increases exponentially with time until it reaches a value $B\sim 2B_{\rm j}$, after that the amplification enters in a non-linear regime and the magnetic field growth becomes linear with time. The distribution of relativistic protons driving the current spans from ≈ 1 GeV to $E_{\rm p,max}\gg$ GeV and therefore the (total) saturated magnetic field $B_{\rm sat}$ immediately upstream of the shock is estimated by considering the total proton population with energy density $U_{p,\rm tot}$ and acceleration efficiency $\eta_{p,\rm tot}$, which gives

$$\frac{B_{\rm sat}}{\rm mG}\sim 0.3\left(\frac{U_{p,\rm tot}}{10^{-6}\,\rm erg\,cm^{-3}}\right)^{\frac{1}{2}}\left(\frac{v_{\rm sh}}{1000\,\rm km\,s^{-1}}\right)^{\frac{1}{2}} \tag{2.2}$$

for fiducial values in MYSO jets. Once the magnetic field strength reaches the saturation value $B_{\rm sat}$, the Alfvén velocity becomes larger and the Larmor radius of particles decreases. Then the NRH instability becomes subdominant.

The condition for efficient magnetic field amplification by the NRH instability is $\Gamma_{\rm max}t > 10$, where the available time t is different for parallel and perpendicular shocks. We consider this relation for constraining the maximum energy of protons in parallel shocks in the termination region of MYSO jets, and in perpendicular shocks in the hotspots of powerful radiogalaxies.

3 MYSO jets

Stars are formed within dense molecular clouds, accreting matter onto the central protostar with the formation of a circumstellar disc and bipolar jets. These jets move with speeds $v_{\rm j}\sim 300-1500$ km s^{-1} into the ambient molecular cloud. For certain combinations of $v_{\rm j}$ and ambient and jet ($n_{\rm j}$) densities, the termination region is composed of an adiabatic reverse shock and a radiative bow shock. This scenario leads to a fast growth of hydrodynamical instabilities and a significant level of mixing. The self-similar dynamics of this configuration of shocks was presented for the first time in Gintrand et al. (2021), whereas its relevance for the gamma-ray emission in protestellar jets and nova outflows was studied by del Valle et al. (2022). The advantage of this configuration of shocks is that, whereas particles are accelerated in the adiabatic shock, the downstream region of the radiative shock acts as a dense target for gamma-ray emission through inelastic proton-proton collisions and relativistic Bremsstrahlung. In addition, the radiation field from the downstream region of the radiative shock can ionise the jet plasma, increasing the efficiency of particle acceleration from the adiabatic shock. This termination region is prone to the growth of hydrodynamic instabilities that are now possible to study through high-energy density laboratory experiments.

The magnetic field in the jet termination region can be amplified by the NRH instability (Araudo et al. 2021). In this case, given that only the most energetic protons can penetrate far upstream from the shock and amplify the magnetic field in the shock precursor, the available time to accelerate these particles is $\sim 10/\Gamma_{\rm max}(E_{\rm p,max})$. We consider the upper limit $R_{\rm j}/v_{\rm rs}$ for the time that protons need to reach the precursor, where $R_{\rm j}$ is the jet width at the termination region and $v_{\rm rs}\sim v_{\rm j}$ is the velocity of the revers shock. By equating $10/\Gamma_{\rm max}(E_{p,\rm max}) = R_{\rm j}/v_{\rm rs}$, the maximum energy of protons is (Bell et al. 2013; Schure & Bell 2014)

$$\frac{E_{p,\rm max}}{\rm m_p c^2} = \begin{cases} 66(2-s)\left(\frac{U_{p,\rm tot}}{10^{-5}\rm erg\,cm^{-3}}\right)\left(\frac{R_{\rm j}}{10^{16}\rm cm}\right)\left(\frac{n_{\rm j}}{10^4\,\rm cm^{-3}}\right)^{-\frac{1}{2}} & s<2 \\ 66\log\left(\frac{E_{p,\rm max}}{\rm GeV}\right)^{-1}\left(\frac{U_{p,\rm tot}}{10^{-5}\rm erg\,cm^{-3}}\right)\left(\frac{R_{\rm j}}{10^{16}\rm cm}\right)\left(\frac{n_{\rm j}}{10^4\,\rm cm^{-3}}\right)^{-\frac{1}{2}} & s=2 \\ \left[\frac{66(s-2)}{m_p c^2}\left(\frac{U_{p,\rm tot}}{10^{-5}\rm erg\,cm^{-3}}\right)\left(\frac{R_{\rm j}}{10^{16}\rm cm}\right)\left(\frac{n_{\rm j}}{10^4\,\rm cm^{-3}}\right)^{-\frac{1}{2}}\right]^{\frac{1}{s-1}} & s>2 \end{cases}. \tag{3.1}$$

Electrons diffuse in the turbulence generated by protons and therefore their maximum energy is $E_{e,\rm max}\leq E_{p,\rm max}$.

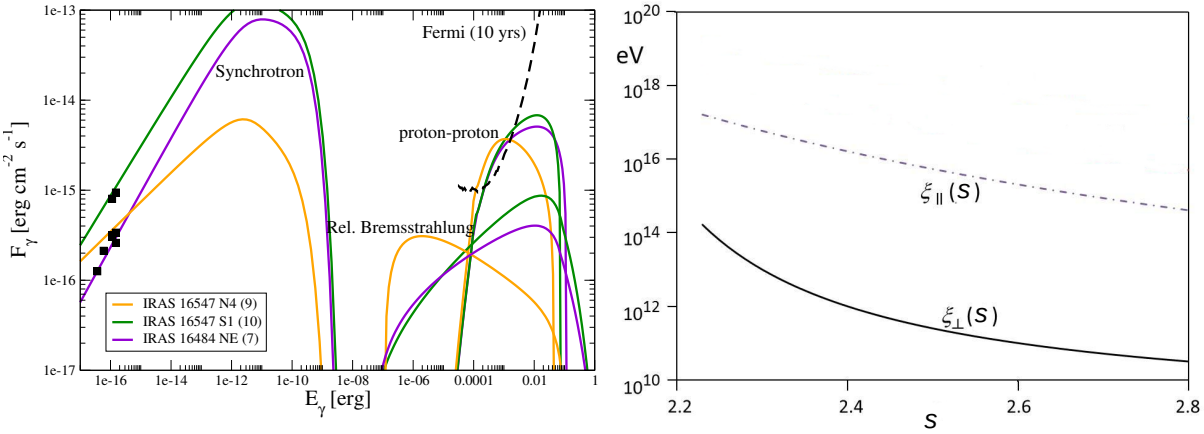

Fig. 2. Left: Spectral energy distribution from radio to gamma-rays. Black squares are the synchrotron data (Purser et al. 2016) and the black dashed line is the Fermi sensitivity for 10 years of observations (Araudo et al. 2021). **Right:** Maximum energy in eV of CR accelerated by a relativistic shock (adapted from Bell et al. 2018).

3.1 Gamma-ray emission

TeV electrons and protons can emit γ-rays by their interaction with ambient cold protons through relativistic Bremsstrahlung and proton-proton collisions. By considering that the density in the non-thermal emitter is $4n_{\rm j}$, Araudo et al. (2021) computed the spectral energy distribution for a sample of eleven non-thermal lobes in jets powered by massive protostars. Among them, the North (N) and South (S) lobes in IRAS 16547-4247 (Araudo et al. 2007) and the NE lobe in IRAS 16484 are potentially detectable by the Fermi satellite, as it is shown in the left panel of Figure 2. Note that the proton-proton collisions and relativistic Bremsstrahlung cooling time is $t_{\rm Br,pp} \propto 1/n$, where n is density in the emitter, and therefore the interaction of relativistic protons with clumps denser than the jet will increase the γ-ray flux.

In del Valle et al. (2022) we show a significant density enhancement in the contact discontinuity due the strong cooling downstream of the bow shock. The layer is unstable and the mixing facilitates the transport of relativistic particles with energies $E_{e,p}$ from the reverse shock (the accelerator) up the region far downstream. We consider for simplicity spatial diffusion with coefficient $D = 10^{25}\,(E_{e,p}/10\,{\rm GeV})^{0.5}\,{\rm cm^2\,s^{-1}}$ (slower than the typical value in the interstellar medium due to the instabilities) and characteristic time $t_{\rm diff}$. By comparing

$$\frac{t_{\rm diff}}{\rm s} \sim 10^7 \left(\frac{R_{\rm j}}{10^{16}\,{\rm cm}}\right)^2 \left(\frac{E_{e,p}}{10\,{\rm GeV}}\right)^{-\frac{1}{2}} \quad \text{and} \quad \frac{t_{\rm Br,pp}}{\rm s} \sim 2\times 10^{11} \left(\frac{n}{10^4\,{\rm cm^{-3}}}\right)^{-1}, \tag{3.2}$$

we can conclude that a significant enhancement in the gamma-ray flux from the jet termination region is expected if $n \gg n_{\rm j}$, as it is the case when the bow shock is radiative and the reverse shock is adiabatic. We note that Yan et al. (2022) found a point-like γ-ray excess in the Fermi database in the direction of the Herbig Haro (HH) objects HH80 and HH81.

4 Hotspots

Radiogalaxies are the subclass of active galactic nuclei in which jets are clearly detected at radio frequencies. Hotspots are usually detected at the jet termination region where electrons accelerated at the reverse shock emit synchrotron emission from radio to optical wavelengths. The synchrotron spectrum turnover at frequency $\sim 10^{14}$ Hz typically observed in the hotspots indicates that the maximum energy of non-thermal electrons is $E_{e,\rm max} \sim 0.2\sqrt{B/100\mu{\rm G}}$ TeV. Motivated by the realization of magnetic field damping in the southern hotspot of the radiogalaxy 4C74.26, Araudo et al. (2015) and Araudo et al. (2016) have explored in depth the physical conditions in the hotspots of a larger number of powerful radiogalaxies and conclude that $E_{e,\rm max}$ cannot be determined by synchrotron cooling, at least the density in the jet termination region is unreasonably large. A similar analysis performed for the primary hotspot in Cygnus A leads to the same conclusion (Araudo et al. 2018). The maximum energy should therefore be determined by a more fundamental limit.

We consider that the magnetic field is amplified by the NRH instability (Bell 2004, 2005) in the reverse termination shock. We assume that a uniform perpendicular magnetic field exists upstream of the jet reverse shock, and it is compressed to a downstream magnitude B_0 as it passes through the shock. Electrons and ions are accelerated in a relativistic quasi-perpendicular shock only if they are strongly scattered within a distance of one Larmor radius $r_{\rm g0} = E/eB_0$ downstream of the shock. The maximum energy $E_{p,\max\perp}$ that particles can achieve when they are accelerated in a perpendicular shock in a magnetic field B_1 amplified by the NRH is determined by the condition $\Gamma_{\max} t > 10$, where $t \sim r_{\rm g0}/c$ is the time in which the plasma advects a distance of $r_{\rm g0}$ in the shock downstream region. The condition $\Gamma_{\max} r_{\rm g0}/c > 10$ leads to

$$\frac{E_{p,\max\perp}}{\rm eV} = \xi_\perp \left(\frac{B_0}{\mu\rm G}\right)^{-\frac{1}{s-2}} \left(\frac{n_{\rm j}}{10^{-4}\,\rm cm^{-3}}\right)^{\frac{1}{2s-4}}, \quad \text{where} \quad \xi_\perp = 10^{\frac{9s-16.8}{s-2}}. \tag{4.1}$$

This analysis assumes that $r_{\rm g0}(E_{p,\max\perp}) = E_{p,\max\perp}/(eB_0) < R_{\rm jet}$. This condition only holds if $B_0 > B_{\rm crit}$, where

$$B_{\rm crit} = \frac{E_{p,\max\perp}}{eR_{\rm j}} = 10^{-\frac{9s-19.2}{s-1}} \left(\frac{R_{\rm jet}}{\rm kpc}\right)^{-\frac{s-2}{s-1}} \left(\frac{n_{\rm j}}{10^{-4}\,\rm cm^{-3}}\right)^{\frac{1}{2s-2}} \mu\rm G. \tag{4.2}$$

When $B_0 < B_{\rm crit}$ the shock behaves as quasi-parallel and the time available for magnetic field amplification is therefore $t = R_{\rm j}/c$. The condition $\Gamma_{\max} R_{\rm j}/c > 10$ leads to a maximum energy

$$\frac{E_{p,\max\parallel}}{\rm eV} = \xi_\parallel \left(\frac{R_{\rm j}}{\rm kpc}\right)^{-\frac{1}{s-1}} \left(\frac{n_{\rm j}}{10^{-4}\,\rm cm^{-3}}\right)^{\frac{1}{2s-2}}, \quad \text{where} \quad \xi_\parallel = 10^{\frac{9s+1.1}{s-1}}. \tag{4.3}$$

In the right panel of Figure 2 we plot $E_{p,\max\parallel}$ and $E_{p,\max\perp}$. These calculations show that hotspots cannot accelerate UHECRs, since $E_{p,\max\perp} \ll 10^{18}$ eV. We conclude that if UHECRs are accelerated by shocks, then the shocks must be mildly relativistic and the magnetic field quasi-parallel.

4.1 UHECRs

Jet plasma slow down after passing through the reverse shock and becomes supersonic again in the sonic surface leading the formation of backflows. The numerical study carried out by Matthews et al. (2019) shows that about 10 per cent of the tracer particles pass through a shock with Mach number $M > 3$ where efficient cosmic-ray acceleration can be expected. More generally, tracer particles pass through more frequently occurring weak shocks with low M. Acceleration in many weak shocks can be described as Fermi II in a turbulent plasma with a turbulence velocity comparable with the large-scale background flow velocity. The rate of Fermi II acceleration is of the same order as that of shock acceleration if the characteristic velocity of the turbulence contributing to cosmic-ray acceleration is comparable to the shock velocity. In this case, the Fermi II process accelerates cosmic rays to the same energy that can be achieved by shock acceleration (Fermi I). We describe here the case of Fermi I acceleration.

Our model for UHECR acceleration at a single shock in the backflows assumes 2D geometry in which the flux tube is infinite and uniform (in the direction parallel to the jet) and a strong shock with speed $v_{\rm sh}$ is located along the flux tube of width l. The shock extension is also l and the magnetic field B is parallel to the shock normal. The diffusion coefficients perpendicular and parallel to the magnetic field are $D_\perp = D_{\rm Bohm}/(\omega_{\rm g}\tau_{\rm scat})$ and $D_\parallel = D_{\rm Bohm}(\omega_{\rm g}\tau_{\rm scat})$, respectively, where the scattering time is $\tau_{\rm scat} > 1/\omega_{\rm g}$, and $\omega_{\rm g}$ is the gyro frequency of particles with energy E. Note that $D_\parallel D_\perp = D_{\rm Bohm}^2$, where $D_{\rm Bohm}$ is the Bohm diffusion coefficient. In Bell et al. (2019) we show that the spectrum of escaping particles extends up to $\sim 0.6E_{\rm Hillas}$, where $E_{\rm Hillas} = ev_{\rm sh}Bl$ is the Hillas energy. We can understand this result by comparing the acceleration time $\tau_{\rm FI} = 20D_\parallel/v_{\rm sh}^2$ with the diffusion loss timescale from the sides of the flux tube $\tau_{\rm diff,\perp} \sim l^2/D_\perp$. By equating $\tau_{\rm FI} = \tau_{\rm diff,\perp}$ we obtain $E_{\max} = 0.35E_{\rm Hillas}$, which is very similar to the value obtained by Bell et al. (2019). Interestingly, $E_{\rm Hillas} \sim 10$ EeV when $v_{\rm sh} = 0.1c$, $l = 1$ kpc and $B = 100\,\mu$G (Matthews et al. 2019) and therefore UHECRs can be accelerated in the backflows of powerful radiogalaxies.

5 Conclusions

We study the jet termination region in MYSO and radiogalaxies. Synchrotron emission from electrons accelerated in the jet reverse shock indicates that the magnetic field must be locally amplified. Motivated by this finding, we consider magnetic field amplification by the NRH instability and constrain the maximum energy

of the particles by imposing the condition that the particles driving the instability must have enough time to amplify the magnetic field before escaping from the acceleration region.

- MYSO. For certain values of the jet and ambient densities, the leading working surface is composed of an adiabatic and a radiative shock. This shock combination is of interest for particle acceleration and subsequent non-thermal radiation. Particles are expected to be efficiently accelerated in strong adiabatic shocks, while the radiative shock produces a strong compression of the plasma. High-energy particles accelerated in the adiabatic shock diffuse up to the dense layer downstream of the radiative shock where they can undergo further re-energization by compression (e.g., Enßlin et al. 2011) and also an enhancement of radiative losses in the denser layer in the form of relativistic Bremsstrahlung for leptons and proton-proton inelastic collisions in the case of hadrons. These results are of great relevance for detectability studies of MYSO jets in the gamma-ray domain.

- Hotspots. We have investigated the physical mechanism that constraints the maximum energy of particles accelerated in the reverse termination shock. By assuming that the shock is quasi-perpendicular, particles cannot diffuse further than a distance r_{g0} downstream of the shock giving a maximum energy $E_{p,\max\perp} \sim 0.1 - 100$ TeV when the steepness of the CR spectrum is $2.2 \leq s \leq 2.8$. It is possible that mildly relativistic parallel, but not perpendicular, shocks might be good UHECR accelerators. We examine the acceleration of cosmic rays in mildly relativistic parallel strong shocks in hydromagnetic flux tubes in the lobes of radio galaxies. We show that the maximum CR energy at a single shock in a flux tube is close to the Hillas energy, offering a suitable environment for the acceleration of UHECRs. Note however that radiogalaxies satisfying the power requirement for accelerating UHECRs are outside the Greisen–Zatsepin–Kuzmin horizon (~ 50 Mpc). In order to reconcile the arrival direction of UHECRs with particles being accelerated in powerful radiogalaxies, Bell & Matthews (2022) proposed that UHECRs detected by the Telescope Array from the direction of M82 and M81 group of galaxies might be the echo of UHECRs emitted by Centaurus A in an earlier more powerful phase (See also Matthews & Taylor 2023).

References

Araudo, A. T., Bell, A. R., & Blundell, K. M. 2015, ApJ, 806, 243
Araudo, A. T., Bell, A. R., Blundell, K. M., & Matthews, J. H. 2018, MNRAS, 473, 3500
Araudo, A. T., Bell, A. R., Crilly, A., & Blundell, K. M. 2016, MNRAS, 460, 3554
Araudo, A. T., Padovani, M., & Marcowith, A. 2021, MNRAS, 504, 2405
Araudo, A. T., Romero, G. E., Bosch-Ramon, V., & Paredes, J. M. 2007, A&A, 476, 1289
Axford, W. I., Leer, E., & Skadron, G. 1977, International Cosmic Ray Conference, 11, 132
Bell, A. R. 1978, MNRAS, 182, 147
Bell, A. R. 2004, MNRAS, 353, 550
Bell, A. R. 2005, MNRAS, 358, 181
Bell, A. R., Araudo, A. T., Matthews, J. H., & Blundell, K. M. 2018, MNRAS, 473, 2364
Bell, A. R. & Matthews, J. H. 2022, MNRAS
Bell, A. R., Matthews, J. H., Blundell, K. M., & Araudo, A. T. 2019, MNRAS, 487, 4571
Bell, A. R., Schure, K. M., Reville, B., & Giacinti, G. 2013, MNRAS, 431, 415
Blandford, R. D. & Ostriker, J. P. 1978, ApJ, 221, L29
del Valle, M. V., Araudo, A., & Suzuki-Vidal, F. 2022, A&A, 660, A104
Enßlin, T., Pfrommer, C., Miniati, F., & Subramanian, K. 2011, A&A, 527, A99
Gintrand, A., Moreno-Gelos, Q., Araudo, A., Tikhonchuk, V., & Weber, S. 2021, ApJ, 920, 113
Krymskii, G. F. 1977, Soviet Physics Doklady, 22, 327
Matthews, J. H., Bell, A. R., Blundell, K. M., & Araudo, A. T. 2019, MNRAS, 482, 4303
Matthews, J. H. & Taylor, A. M. 2023, arXiv e-prints, arXiv:2301.02682
Purser, S. J. D., Lumsden, S. L., Hoare, M. G., et al. 2016, MNRAS, 460, 1039
Schure, K. M. & Bell, A. R. 2014, MNRAS, 437, 2802
Yan, D.-H., Zhou, J.-N., & Zhang, P.-F. 2022, Research in Astronomy and Astrophysics, 22, 025016